



Seaweed ingress of cooling water intakes with predictions for Torness power station

Nikolaos Spanakis¹ · Peter K. Stansby¹ · Benedict D. Rogers¹ · Pietro Bernardara²

Received: 27 February 2021 / Accepted: 7 September 2021 / Published online: 30 September 2021
© The Author(s) 2021

Abstract

Seaweed ingress into the cooling water intakes of nuclear power stations has caused several disruptions to electricity supply. Seaweed is transported by tidal and wave-induced currents after dislodgement from the sea bed following stormy conditions but ingress will be shown to be not only determined by wave conditions. An integrated model system has been developed to predict such ingress and applied at the Torness power station in Scotland where the mass of seaweed recovered was measured for some ingress cases. Prior to each case, seaweed is assumed initially to be distributed in areas surveyed within the surrounding coastal domain with a mass per unit area based on local measurements. Criteria for dislodgement are based on near-bed velocity. Six cases where the mass of ingress was measured and two cases with no ingress have been modelled and predicted by adjusting a dislodgement factor (a multiplier on the threshold velocity) within a relatively narrow range.

Keywords Coastal hydraulics · Cooling water intakes · Seaweed dislodgement · Seaweed ingress · Electricity supply disruption

1 Introduction

Dislodgement of seaweed by storm waves and subsequent transportation by currents may cause ingress into the cooling water intakes of power plants and blocking if the accumulated volume cannot be removed quickly enough; this can disrupt the generation of electrical power. Stations may even temporarily be shut down if cooling capacity is insufficient for the steam cycle which drives the turbines. We consider the Torness power station on the eastern coast of Scotland in Skateraw Bay where the surrounding region is rocky and populated with many different species of seaweed including kelp and red algae. Prediction of seaweed ingress is thus highly desirable. Seaweed may have been recently dislodged in a storm or it may have been drifting (and decaying) for days or weeks. A dislodgement model is proposed and seaweed transport is predicted through hydrodynamic modelling.

Torness power station delivers over 1000 MW of electricity from two advanced gas-cooled reactor (AGR) units.

Figure 1 shows an aerial view from Google Earth. The water intake and the channel are visible at the shoreline in front of the station. This configuration is unprotected from waves from the North, as the breakwater is located at the eastern end of the bay. The location is in an open coast domain where the hydrodynamics are driven by tides and waves and occasionally storm surges.

Seaweed is attached to the seabed through a holdfast from which fronds emerge. The typical morphology of seaweed consists of a stem-like stipe and fleshy blades. The holdfast and fronds together form the thallus. Figure 2 shows the seaweed components. Elongated, irregularly corrugated blades branch off one side of each stipe at intervals.

During winter storms 10–90% of the intertidal and shallow subtidal population of seaweed is thought to break away (Hansen and Doyle 1976; Dyck and BeWreede 2006a, b). The dislodgement of seaweed in its natural environment is dependent on many parameters such as size, age, substratum where the holdfast is attached, and flexibility (Denny and Gaylord 2002; Thomsen 2004; Martone et al. 2012; Mach et al. 2011; Bekkby et al. 2014). Seaweed is also known to change its form and size adapting to environmental conditions while growing (Blancette 1997; Kawamata 2001). Wernberg and Thomsen (2005) collected data from 30 different studies assessing the breaking force required to dislodge

✉ Peter K. Stansby
p.k.stansby@manchester.ac.uk

¹ School of Engineering, University of Manchester, Manchester, UK

² EDF Energy R&D, London, UK

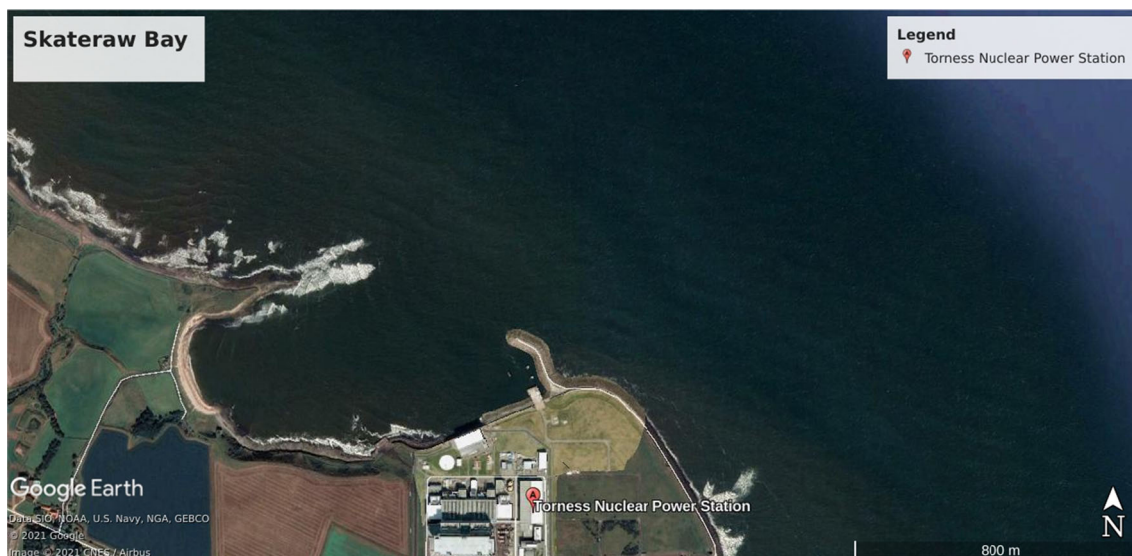


Fig. 1 Torness Power Station located as Skateraw Bay (Google Earth)

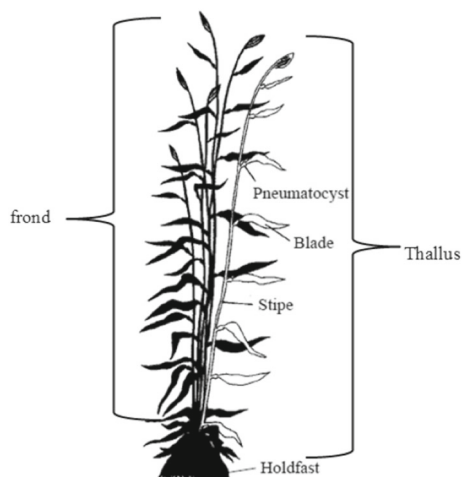


Fig. 2 Representative seaweed components from Utter and Denny (1996)

seaweed and its respective thallus area for a variety of seaweed species. Wernberg and Thomsen concluded that there is a strong relation between the area of the thallus and the force required to dislodge the seaweed. Denny (1995) described the hydrodynamic forces imposed by the wave-induced water motion on the seaweed characterising drag, lift and acceleration (inertia). Despite the effect of size on inertia force, Denny (1995) stated that under all but the most severe wave conditions and for all but the largest seaweed, the effect of inertia force is small compared to the drag force. The velocities close to the bed due to waves determine drag force, and dislodgement occurs above a certain limit. This enables identification of wave conditions in terms of wave height and period for a given depth causing seaweed dislodgement.

The system from seaweed dislodgement to cooling water ingress is thus complex and coupled, covering a large coastal domain. Highly resolved modelling of each component is not computationally practical and precise conditions are difficult to define, e.g. due to seasonal variation in seaweed and seabed conditions, wave conditions with directionality and current interaction. The policy is thus to undertake relatively simple modelling with spectral wave modelling, depth-averaged current modelling, a simple formula for velocity due to breaking waves and an empirical dislodgement formulation. The intention is to calibrate with ingress data measured over 8 years with criteria as simple as possible to assess the practicality and efficacy of a prediction method. Such ingress data have not been presented previously to our knowledge.

In this paper, the trajectories of seaweed causing ingress at the cooling water intake are determined after dislodgement from surveyed seaweed banks in the surrounding coastal area (AMEC 2014). The seaweed particulate, represented as discrete masses, is tracked to determine which reach the intake. Related studies have previously been conducted for different applications. Filippi et al. (2010) developed a model for tracking drifting seaweeds in ocean currents using the Princeton Ocean circulation Model (POM). In the present methodology the tidal currents are simulated in computationally efficient depth-averaged form using the open source code TELEMAC-2D and the wave propagation using the spectral wave model TOMAWAC. Wave-induced radiation stresses from TOMAWAC are input to TELEMAC-2D to give tidal and wave-induced currents combined.

The paper is organised as follows: First the probability of events is correlated with wave height from a wave buoy in the coastal region; this shows that although the likelihood of an event increases as wave height increases the correla-

Table 1 Ingress cases and associated $H_{s,0}$, occurrence and probability

Event	$H_{s,0}$	Occurrences with $H_s \geq H_{s,0}$	Event probability with $H_s \geq H_{s,0}$
25/09/2012	6.68	4	0.25
24/12/2012	6.03	10	0.20
20/11/2016	5.96	13	0.23
06/09/2008	4.24	51	0.078
18/11/2015	4.18	57	0.087
24/05/2013	3.80	86	0.070
24/09/2010	3.67	94	0.074

tion is low. Prediction requires process modelling which is then described for tidal flows and wave propagation with validation from field measurement. Wave-induced kinematics, seaweed dislodgement criteria and transport are then described. The model system is then applied to eight cases for the Torness power station and ingress is compared with measured data and three non-events with large waves. Electricity supply was disrupted for three of these events. The complexity and effective calibration of the model system is discussed and finally some conclusions are made.

2 Dependence on wave climate

It has been observed by Torness power station managers that ingress events are more likely in stormy weather. The position of the power station in the coastal domain is shown in Fig. 3 with the positions of measuring stations for hydrodynamic validation.

There have been seven events with significant ingress since 2008 that either caused drop of load or shutdown or were managed successfully by station staff, listed in Table 1. $H_{s,0}$ is the daily maximum significant wave height within the day before the incident measured from Isle of May wave buoy. As expected the $H_{s,0}$ cumulative probability fits a log normal distribution. The number of daily maximum values that exceeded $H_{s,0}$ since 2008 are shown in Table 1. As larger wave heights occurred from the open sea with directions from north-west to north east only those were recorded.

This shows that the ingress is more likely with larger wave heights with a maximum 1:4 likelihood for $H_{s,0} > 6$ m and a maximum 1:11 likelihood for $H_{s,0} < 4.24$ m with small variation to 3.67 m. The number of data points is obviously small and there is not an obvious distribution formula but it is clear that wave height is not the only criterion for an event happening. Process modelling is necessary to include all factors involved and this is undertaken in the rest of this paper.

2.1 Coastal area hydrodynamics

The tidal flows are modelled using the TELEMAC-2D finite-element code with offshore boundary conditions taken from a continental shelf model CS20 of the National Oceanography Centre (NOC) in the U.K. (ABPmer 2008). With the resulting surface elevations the wave climate is modelled using the spectral model TOMAWAC with offshore wave boundary conditions from the CEFAS buoy at the Isle of May and the wind conditions from the nearby nearshore meteorological station (Leuchars, see Fig. 3). The radiation stresses from TOMAWAC are then added to TELEMAC-2D so that wave-induced currents are included. The effect of currents on waves is not considered significant following investigations for a similar open coast domain (Kuang and Stansby 2004). The TELEMAC-2D flow module solves the shallow water equations (depth-averaged momentum and continuity), with the depth-averaged $k - \epsilon$ turbulence model for horizontal diffusion and source terms for Coriolis force and radiation stresses from TOMAWAC. The numerical scheme includes a choice of several discretisation options for advection terms (Hervouet 2007). In this study, the classical N scheme was used for velocity, the PSI scheme for surface elevation and characteristics for $k - \epsilon$. TOMAWAC models directional spectra by solving the propagation equation for wave action on a finite-element grid (Benoit 2002) predicting the wave climate defined by significant wave height, direction and mean wave period. The combined use of TOMAWAC and TELEMAC-2D with a stochastic transport algorithm for seaweed, specifically algal bloom (Joly 2014) provides a framework for predicting seaweed transport. The coastal domain extends approximately 10 km in the cross shore direction and 22 km alongshore with bathymetry as shown in Fig. 4; the power station is located near the centre of the Southern boundary which represents the coastline. The mesh size varies from 300 m offshore to 10 m close to the water intake. The mesh used herein consists of 34,917 nodes and 68,472 elements as shown in Fig. 5. The time series of water level and velocity components at each point on the model boundary are input from the model CS20 which has a regular grid with a resolution of 1.8 km and represents the tidal propagation generated by 15 tidal components. With a representative Nikuradse roughness height of 0.22 m the surface elevations showed close agreement with measurements at five locations within the domain, whereas velocities slightly underestimated the measured values as shown in Fig. 6 for the SEPA location (see Fig. 3).

The same mesh is used for wave modelling. The offshore boundary conditions were provided by the WaveNet buoy of the Isle of May (shown in Fig. 3). The values of peak wave period, peak wave direction, wave directional spread and significant wave height, were extracted from the buoy provided by CEFAS (<http://wavenet.cefas.co.uk/Map>) and used as off-

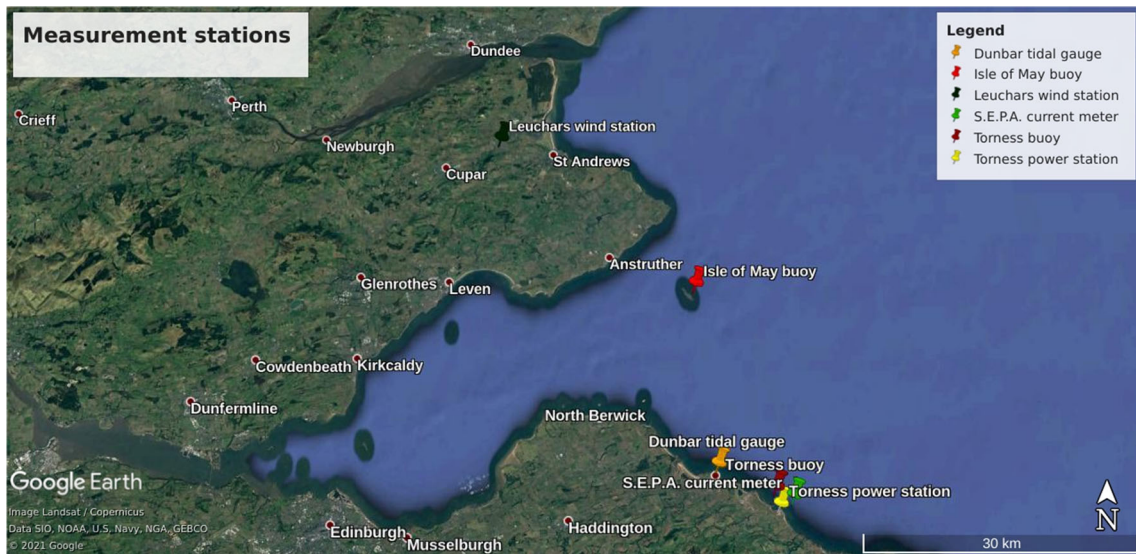


Fig. 3 The position of the power station in the coastal domain showing the position of measurement stations for validation of the coastal hydrodynamic model: Dunbar port (tidal gauge), Isle of May CEFAS wave

buoy (offshore wave climate), Torness Buoy (nearshore wave climate), Scottish Environmental Protection Agency (SEPA) current meter and Leuchars wind station. (from Google Earth)

Fig. 4 Bathymetry of coastal domain around Torness Power Station

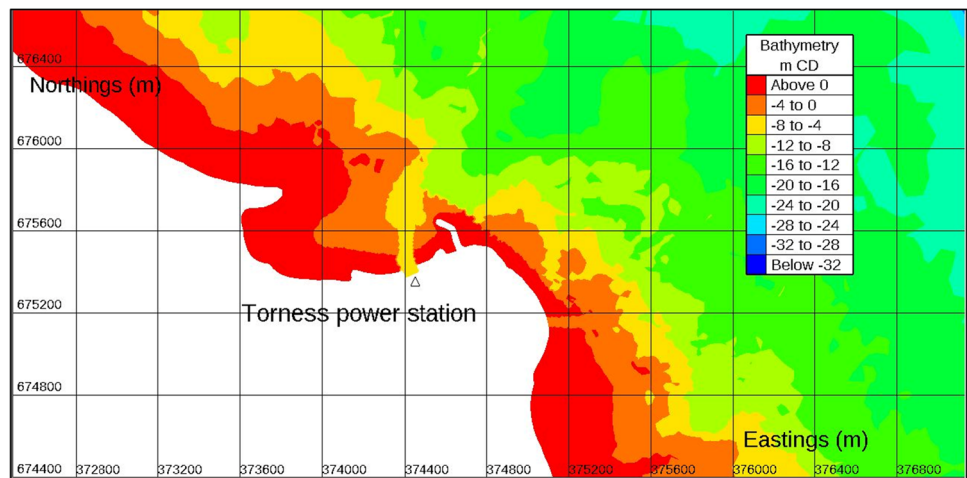


Fig. 5 Computational mesh for coastal domain

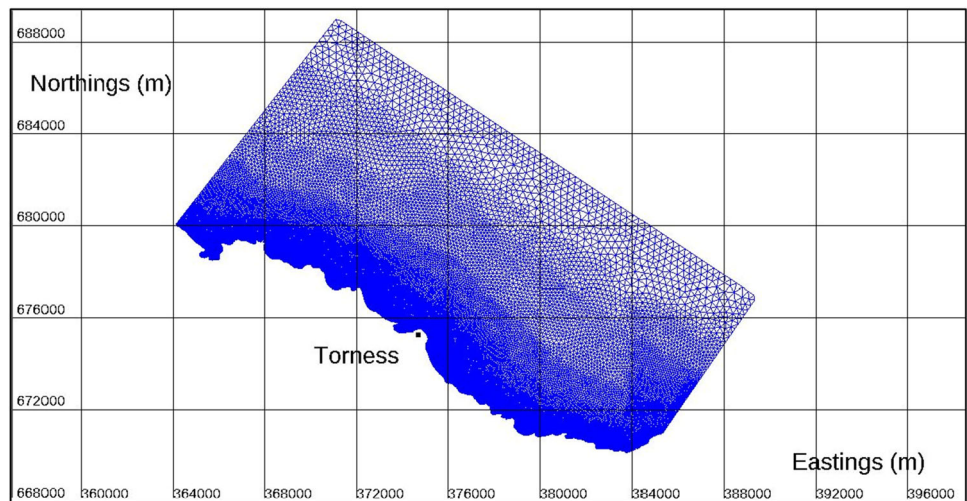


Fig. 6 Comparison of velocity: U component at top and V component at bottom, between model (–) and data provided from the Scottish Environmental Protection Agency in 2003 shown by red dots (Potapova-Crighton 2003) at the position shown in Fig. 3

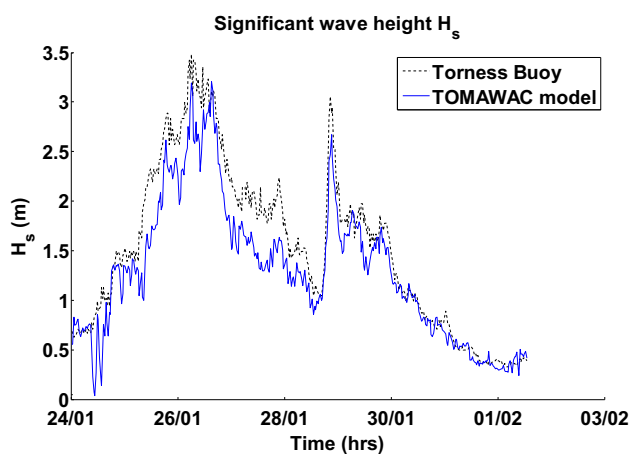
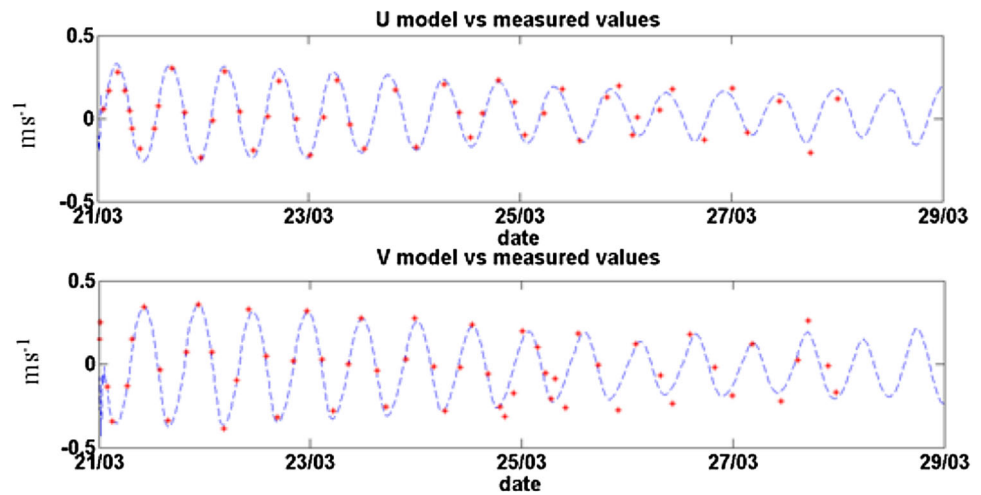


Fig. 7 Comparison of measured and computed significant wave height time history at Torness Buoy for period from 24–01 to 01–02 in 2015

shore boundary conditions. The bathymetry-induced wave breaking criterion of Battjes and Janssen (1978) was used. Comparisons of computed and measured significant wave height and mean direction are shown in Figs. 7 and 8 for a period in 2015 to be reasonable with mean errors of 15.74% and 5.66%, respectively.

2.2 Wave kinematics

The wave climate is computed in time bins of half an hour and is categorised as non-breaking or breaking using the Battjes and Janssen model (1978) with the fraction of breaking waves (Q_{br}) set to 99.5% as predominantly depth-limited with most waves breaking. For each time bin the significant wave height H_s and the mean (zero-crossing) period T_z are used to define the bed velocity for dislodgement. Since dislodgement occurs mainly for breaking waves which are depth-limited, use of a single wave height is considered an acceptable approximation. For non-breaking waves the bed velocity is given

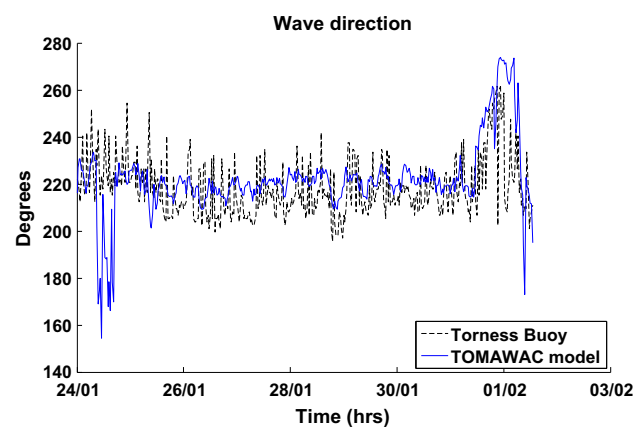


Fig. 8 Comparison of measured and computed wave direction time history at Torness Buoy for period from 24–01 to 01–02 in 2015

simply by linear theory as $u = (\pi H_o/T)/\sinh(kd)$ where T is the wave period (s), H_o is the unbroken wave height (m), k is the wave number and d is water depth (m). For breaking waves which satisfy the shallow water condition the approximation for a solitary wave is appropriate and given as a proportion of the wave speed $\sqrt{g(d+H)}$ (Munk 1949) where g is the acceleration of gravity, 9.81 m/s^2 , and here H is typically a proportion of d equal to 0.7 in this case. The water particle velocity $u = 0.3\sqrt{g(d+H)}$ where the factor 0.3 is for limiting (breaking) wave steepness (Denny 1995) and is consistent with velocity measurements in Seelam et al. (2011). The velocity for dislodgement is assumed to be due to waves only as the current velocity near the bed will be small, in theory zero at the bed. The boundary layer thickness due to breaking waves is uncertain over flexible vegetation such as seaweed and the above formula is an approximation for velocity near the bed. We will use this formula but will calibrate with a multiplying factor to give the ingress mass measured.

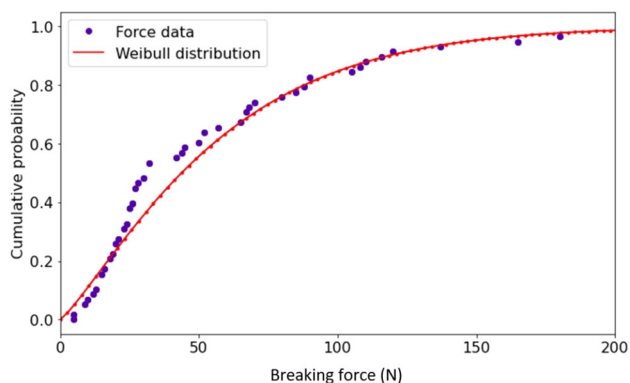


Fig. 9 Cumulative probability of dislodgement as a function of imparted force based on AMEC (2014) data

2.3 Seaweed dislodgement criteria

Seaweed dislodgement forces and density (wet mass per unit area) were measured in the intertidal zone around Skateraw Bay in a survey in September 2014 by AMEC (2014) followed by another survey in January 2015 within a distance of 1.6 km of the cooling water intake. 58 samples were tested and the cumulative probability of dislodgement, for given imparted force, is shown in Fig. 9, which is close to a Weibull distribution. For force greater than 210 N, 100% of seaweed was dislodged. The force exerted by wave action f_d is determined by a drag coefficient C_d such that

$$f_d = 1/2 \rho C_d u^{\beta_d} S_{d,pr} A_{pr},$$

where β_d is the velocity exponent, ρ is the density of water, $S_{d,pr}$ is the shape coefficient of drag, u is water velocity, A_{pr} is the seaweed area projected on to a plane perpendicular to the direction of water motion. General drag coefficients have been determined not accounting for flexibility and a value of 0.1 with $\beta_d = 2$ and $S_{d,pr} = 1$ was found by Johnson and Koehl (1994) and Kawamata (2001). If flexibility is taken into account higher values of C_d will result but motion of the seaweed is also needed (Paul et al 2016) which is not generally known. To determine the projected area for a given wet mass of seaweed, the ratio of 9.8 cm²/g (0.98 m²/kg) has been suggested by Thomsen (2004) and is used here. With this information the probability distribution of force may be converted into a probability distribution of velocity for dislodgement P as shown in Fig. 10 which is close to a log-normal distribution.

$$P = \frac{1}{2} \left(1 + \operatorname{erf} \left[\frac{\ln(u) - \mu}{\sqrt{2}\sigma} \right] \right),$$

where μ is the mean of $\ln(u)$, σ is the variance with $\mu = 1.17$ and $\sigma = 0.50$ giving the fit shown in Fig. 10. The average wet mass of seaweed per unit area measured was 0.34 kg/m² in

summer and 0.14 kg/m² in winter. Summer corresponds to May to November and winter to December to April inclusive. This is distributed uniformly in the seaweed areas, shown in Fig. 11 for (a) summer and (b) winter. The cumulative probability of mass dislodged as function of velocity may be determined and is shown in Fig. 12 for (a) summer and (b) winter conditions with a range of multiplying factors on threshold velocity for calibration. The process model is started 4–14 days prior to an event and dislodgement is activated at half hourly intervals. It is assumed that the velocity causing a particular breaking force dislodges seaweed for that particular force/velocity and smaller values. Basically, seaweed is snapped off as soon as the breaking force is applied. It is not assumed to be a gradual process. It is further assumed that in each half hour time interval only velocities higher than in previous intervals can dislodge more seaweed and that the mass dislodged is the difference between that associated with the higher velocity and the preceding lower velocity. The total mass dislodged cannot exceed the mass available prior to an event.

The dislodged seaweed is then transported using the advection scheme for particles available in TELEMAC-2D, previously applied to algae blooms. This is based on Joly (2011, 2014) with one-way fluid-to-particle coupling with turbulence represented by a stochastic Lagrangian turbulence model. The Simplified Langevin model was used although stochastic effects were found to be minimal. Results were unaffected by the choice of algal type. The seaweed is assumed to be initially uniformly distributed in the mesh cells on the seaweed banks found on the survey in the coastal domain prior to an event.

3 Prediction of ingress

There have been three events when seaweed ingress led to temporary or partial shutdown, reported to occur following adverse weather conditions. To predict this the current-wave model is run from 4 to 14 days before the event to approximately 12 h after.

We also consider other storm conditions when the ingress was measured. The list of conditions in chronological order is shown in Table 2. For cases 1, 2 and 5 shutdown occurred. For case 3 with no shutdown there is small ingress with a low wave height while for case 6 ingress is negligible although wave height is large. For cases 4 and 7 ingress is significant but there was no shutdown. Case 8 was recorded as an event, possibly due to the large wave height, but ingress was not measured.

Ingress is dependent on many factors but we assume that hydrodynamic wave and current modelling is valid and consider sensitivity to threshold dislodgement velocity with velocity defined by simple formulae. Breaking is assumed to

Fig. 10 Cumulative probability of dislodgement as a function of velocity

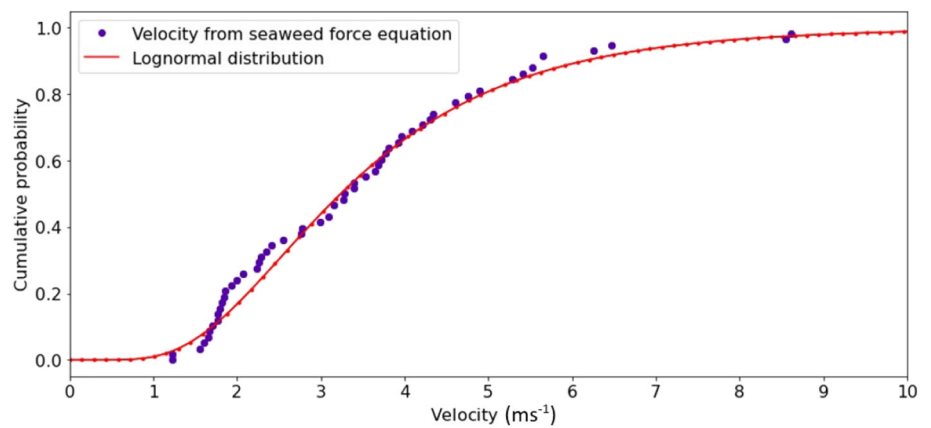
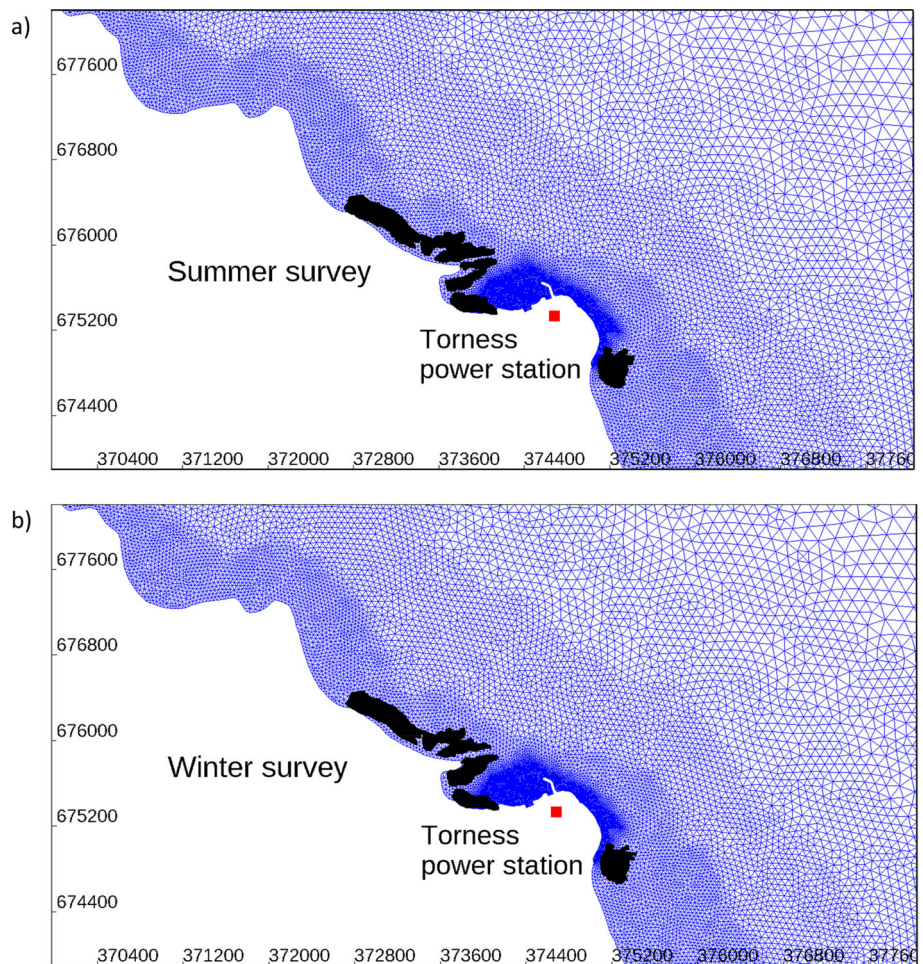


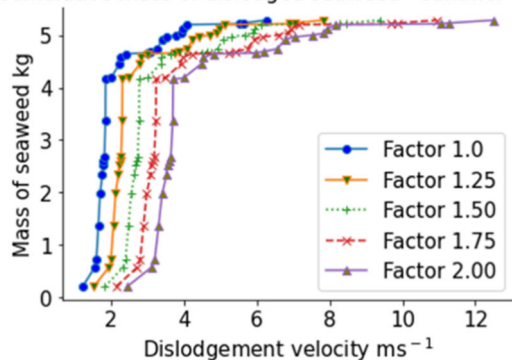
Fig. 11 Seaweed release areas shown by black dots in the computational domain from **a** summer survey, **b** winter survey



be always occurring as we are mainly concerned with storm conditions when breaking will be depth limited; the standard breaking index (wave height/depth) of 0.7 is assumed. We thus tune the dislodgement to give the measured ingress only through a multiplier on the dislodgment velocity shown in Fig. 12, called the dislodgement factor. Cases 1 and 3 are used to demonstrate the results.

Figure 13 shows the surface elevation (with a tidal cycle), wave height and direction and the event time. Figure 14 shows the cumulative ingress with different dislodgement factors. The ingress matches that measured with dislodgement factor between 1.25 and 1.5 with linear interpolation giving 1.47. This process was undertaken for all events and the example of case 3 with small ingress is shown in Figs. 15 and 16 (cor-

a) Cumulative mass of dislodged seaweed - summer survey



b) Cumulative mass of dislodged seaweed - winter survey

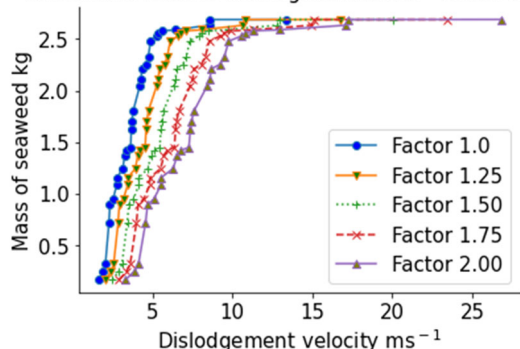


Fig. 12 Cumulative mass of seaweed dislodged per releasing point as a function of dislodgement velocity for **a** summer and **b** winter conditions for different velocity dislodgement factors

responding with Figs. 13 and 14). The dislodgement factor for all cases is given in Table 3 with ingress mass.

The dislodgement factor can be seen to vary between 1.36 and 1.89 which is a small range for such a complex process with simplified modelling. The time of year may influence this factor. The highest value occurs in winter for case 7. Values for cases 1–6 are in range 1.36–1.5 with an average of 1.45 but occur at times throughout the year. There is thus no evidence of seasonality, apart from the density available. The overall average is 1.51. Another factor is the recent storm history as previous mass dislodged will determine seaweed available to be dislodged but this is not taken into account.

4 Discussion

While generally associated with storms, the ingress event with the largest wave height within one day has only a 25% probability of occurrence for a wave height of that magnitude or greater. The prediction of ingress is dependent on a number of coupled physical and bio-mechanical processes. The hydrodynamic modelling for currents and waves is well tried and tested although with some uncertainty. The available mass density and areas of seaweed are assessed from

a site survey, assumed valid through the decade of investigation. The force on the seaweed for dislodgement is based on sample testing, again assumed valid through the decade. It is assumed that a proportion of seaweed is snapped free when a particular force is reached. This is an idealisation as it is likely to be a gradual process in practice, like the elastic yield strength being reached before the ultimate yield strength in structural engineering terms. This gives the velocity required for a proportion of mass dislodgement which is provided by a lookup data base for depth-limited breaking waves. The dislodgement ceases naturally when the available mass is reached. The components of the system model are thus quite standard and calibrated as far as possible but the errors associated with each are uncertain. Inevitably there are errors in the predicted ingress and to match measured ingress a simple multiplier is applied to the dislodgement velocity, referred to as dislodgement factor. This is always greater than unity indicating that the dislodgement velocity is greater than that idealised. There are several possible reasons. The wave heights may be underestimated and there is some evidence to suggest this may be the case, e.g. Fig. 7. The assumed drag coefficient may be too small due to shielding in a seaweed mass or flexibility presenting a more streamlined surface to the flow thus requiring a larger velocity to compensate. The strength of seaweed in situ may be different when transferred to a laboratory for testing. Determining the error associated with each model component and the cumulative effect with other errors is not practical. Fortunately system level calibration based on measured ingress was possible. The single calibration factor for dislodgement velocity was considered to be within quite a narrow band for such a complex system providing a valuable method for predicting ingress thus informing power station operation. However this does depend on knowledge of the location and mass seaweed available from site surveys.

5 Conclusions

A system model combining coastal tidal current and wave simulation, seaweed dislodgement and transport has been developed to predict seaweed ingress into the cooling water intake of power stations. This can affect many power stations around the world. Ingress events at the Torness nuclear power station in Scotland have been predicted where there have been five disruptions to power supply in the last decade. Coastal domain modelling for tides and waves using TELEMAC-2D and TOMAWAC software respectively has been validated against available tidal elevation, current velocity and wave data. Seaweed location and mass distribution in the coastal domain had been surveyed and samples tested to give dislodgment force. The process model is started 4–14 days prior to an event and dislodgement is activated at half hourly inter-

Table 2 Cases with ingress modelled

Case	Date/time	Max H_s (m)	Main wave direction	Seasonal biodiversity	Measured ingress (tonnes)	Recorded event	Partial shutdown
1	06/09/2008 16:14	4.24	East NE	N/A	15.44	Yes	Yes
2	24/09/2010 01:00	3.67	North east	N/A	23.01	Yes	Yes
3	13/06/2012	2.80	East	Summer	4	No	No
4	13/12/2012	6.03	East	Winter	22	Yes	No
5	24/05/2013 03:09	2.93	East	N/A	19.07	Yes	Yes
6	15/03/2015	6.00	East	Winter	None	No	No
7	18/11/2015	4.18	North	Summer	15	Yes	No
8	20/11/2016	5.96	East	Summer	n/a	Yes	No

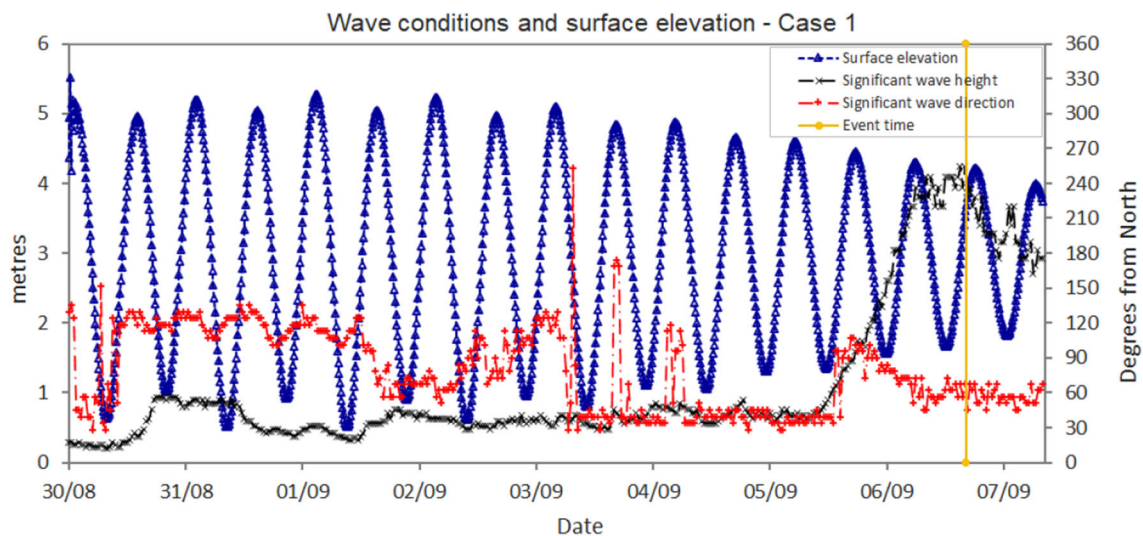
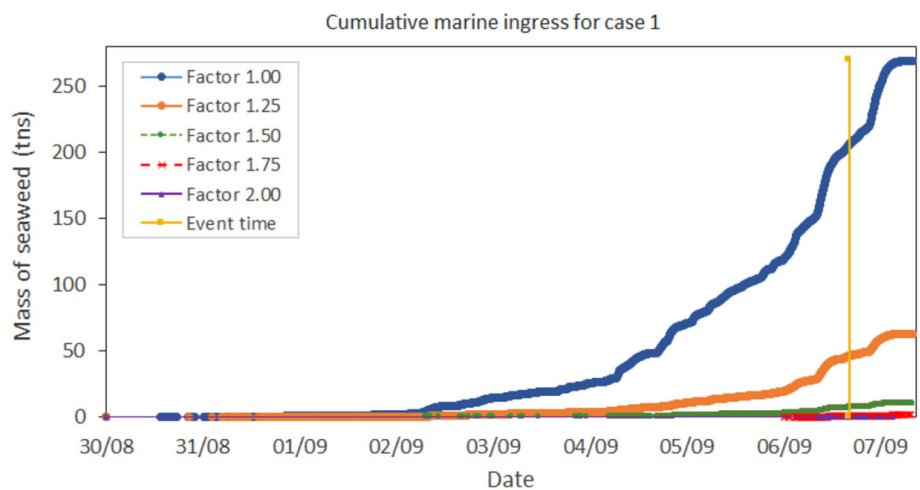


Fig. 13 Wave height and direction, surface elevation for case 1

Fig. 14 Cumulative ingress mass for different dislodgement factors for case 1



vals. The velocity acting on the seaweed is based on the simple solitary-wave formula defined by significant wave height, mean period and depth for breaking waves. It is assumed that in each interval only velocities higher than in previous intervals can dislodge more seaweed and that

the mass dislodged is the difference between that associated with the higher velocity and the preceding lower velocity. The total mass dislodged cannot exceed the mass available prior to an event. A dislodgement factor multiplier on the threshold velocity is introduced to match modelled ingress mass to

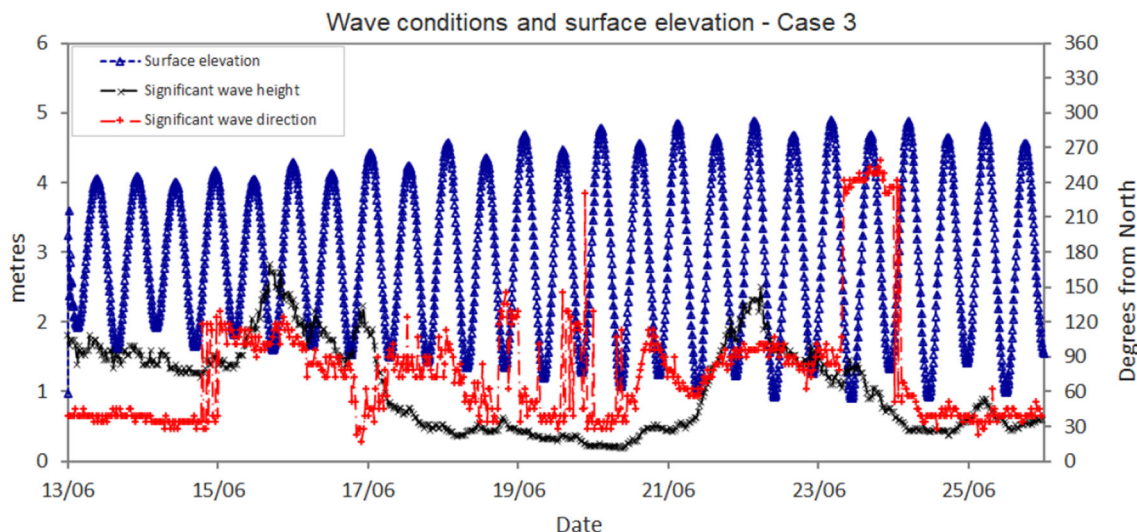


Fig. 15 Wave height and direction, and surface elevation for case 3 (event 3)

Fig. 16 Cumulative ingress mass for different dislodgement factors for case 3 (event 3)

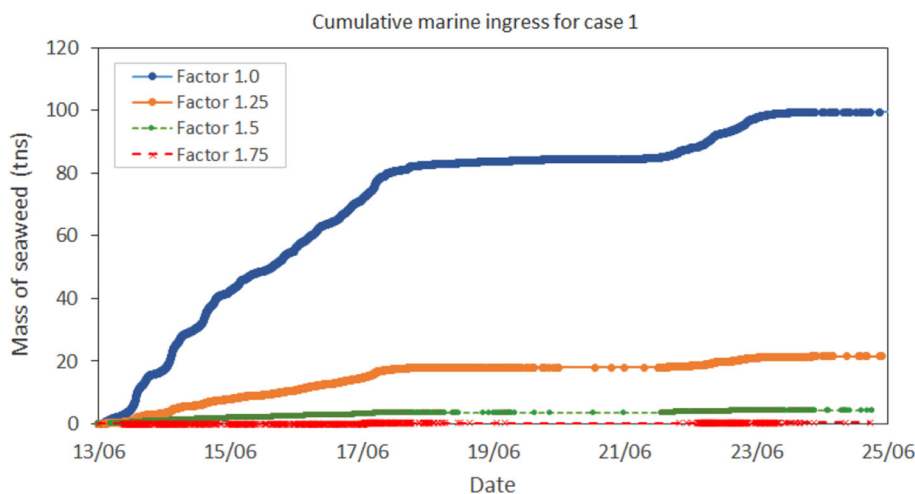


Table 3 Dislodgement factors with ingress mass for each case

Case	1	2	3	4	5	6	7	8 ^a
Ingress mass	15.44	23	4	22	19	0	15	0–8
Dislodgement factor	1.474	1.365	1.5	1.422	1.46	1.5	1.89	1.9–1.3

^aCase 8 was recorded as an event but ingress was not measured. A low dislodgement factor of 1.3 gives an ingress of 8 tonnes and a high value of 1.9 gives no ingress. Small ingress is consistent with an ‘event’.

that measured. This varies in the range 1.36–1.89 with a mean of 1.51 which is considered to be usefully narrow for such a complex system with inputs determined by environmental conditions. For six cases the range is narrower, between 1.36 and 1.5 with a mean of 1.45. Overall, the model is able to predict when there will and will not be seaweed ingress in the cooling water intake providing valuable insight into the conditions leading to a power station shutdown.

Acknowledgements The authors would like to thank the UK Engineering and Physical Sciences Research Council (EPSRC) and EDF Energy for the funding of this project through the Impact Acceleration Account

(IAA) at the University of Manchester and for providing information on the past ingress events. Angus Bloomfield of EDF Energy provided coordination. Some preliminary results were presented in Spanakis et al. (2014) at the Telemac User conference. This work was funded through EPSRC Grant no. IAA 085.

Open Access This article is licensed under a Creative Commons Attribution 4.0 International License, which permits use, sharing, adaptation, distribution and reproduction in any medium or format, as long as you give appropriate credit to the original author(s) and the source, provide a link to the Creative Commons licence, and indicate if changes were made. The images or other third party material in this article are included in the article’s Creative Commons licence, unless indicated otherwise in a credit line to the material. If material

is not included in the article's Creative Commons licence and your intended use is not permitted by statutory regulation or exceeds the permitted use, you will need to obtain permission directly from the copyright holder. To view a copy of this licence, visit <http://creativecommons.org/licenses/by/4.0/>.

References

- ABPmer (2008) Atlas of UK Marine Renewable Energy Resources: Technical Report. R.1432
- AMEC (2014) "Torness Benthic Survey & Habitat Mapping" and the report number is 2014-1022-Report 01
- Battjes JA, Janssen JPFM (1978) Energy loss and set-up due to breaking of random waves. In: Proceedings of the 16th international conference on coastal engineering, Hamburg, Germany, pp 569–587. <https://doi.org/10.9753/icce.v16.32>
- Bekkby T, Rinde E, Gundersen H, Norderhaug KM, Gitmark JK, Christie H (2014) Length, strength and water flow: relative importance of wave and current exposure on morphology in kelp *Laminaria hyperborean*. Mar Ecol Prog Ser 506:61–70. <https://doi.org/10.3354/meps10778>
- Benoit M (2002) TOMAWAC software for finite element sea state modelling—Release 5.2 theoretical note. HP-75/02/065/A (available from HR Wallingford, Oxfordshire, UK)
- Blanchette CA (1997) Size and survival of intertidal plants in response to wave action: a case study with *Fucus gardneri*. Ecology 78:1563–1578
- Denny M (1995) Predicting physical disturbance: mechanistic approaches to the study of survivorship on wave-swept shores. Ecol Monogr 65:371–418. <https://doi.org/10.2307/2963496>
- Denny M, Gaylord B (2002) The mechanics of wave-swept algae. J Exp Biol 205:1355–1362
- Dyck LJ, DeWreede RE (2006a) Reproduction and survival in *Mazzaella splendens* (Gigartinales, rhodophyta). Phycologia 45:302–310. <https://doi.org/10.2216/04-80.1>
- Dyck LJ, DeWreede RE (2006b) Seasonal and spatial patterns of population density in the marine macroalga *Mazzaella splendens* (Gigartinales, rhodophyta). Phycol Res 54:21–31. <https://doi.org/10.1111/j.1440-1835.2006.00405.x>
- Filippi J-B, Komatsu T, Tanaka K (2010) Simulation of drifting seaweeds in East China Sea. Eco Inform 5:67–72. <https://doi.org/10.1016/j.ecoinf.2009.08.011>
- Hansen JE, Doyle WT (1976) Ecology and natural history of *Iridaea Cordata* (Rhodophyta; gigartineae): population structure. J Phycol 12:273–278. <https://doi.org/10.1111/j.1529-8817.1976.tb02844.x>
- Hervouet J-M (2007) Hydrodynamics of free surface flows: modelling with the finite element method. Wiley, Hoboken
- Johnson AS, Koehl MAR (1994) Maintenance of dynamic strain similarity and environmental stress factor in different flow habitats: Thallus allometry and material properties of a giant kelp. J Exp Biol 195:381–410
- Joly A (2011) Modelisation of the diffusive transport of algal blooms in a coastal environment using a stochastic method, in LHSV—Laboratoire Hydraulique Saint Venant, École doctorale Sciences, Ingénierie et Environnement (Paris-Est), Paris
- Joly A (2014) Adding a particle transport module to Telemac-2D with applications to algae blooms and oil spills. EDF R&D, National Hydraulics and Environmental Laboratory, Chatou, France
- Kawamata S (2001) Adaptive mechanical tolerance and dislodgement velocity of the kelp *Laminaria japonica* in wave-induced water motion. Mar Ecol Prog Ser 211:89–104. <https://doi.org/10.3354/meps211089>
- Kuang CP, Stansby PK (2004) Efficient modelling for directional random wave propagation inshore. ICE J Marit Eng 157(MA3):123–131. <https://doi.org/10.1680/maen.2004.157.3.123>
- Mach KJ, Tepler SK, Staaf AV, Bohnhoff JC, Denny W (2011) Failure by fatigue in the field: a model of fatigue breakage for the macroalga *Mazzaella* with validation. J Exp Biol 214:1571–1585. <https://doi.org/10.1242/jeb.051623>
- Martone PT, Kost L, Boller M (2012) Drag reduction in wave-swept seaweed: alternative strategies and new predictions. Am J Bot 99:806–815. <https://doi.org/10.3732/ajb.1100541>
- Munk WH (1949) The solitary wave theory and its application to surf problems. Ann N Y Acad Sci 51:376–424. <https://doi.org/10.1111/j.1749-6632.1949.tb27281.x>
- Paul M, Franziska Rupprecht F, Möller I, Bouma TJ, Spencer T, Kudella M, Wolters G, vanWesenbeeck BK, Jensen K, Miranda-Lange M, Schimmels S (2016) Plant stiffness and biomass as drivers for drag forces under extreme wave loading: a flume study on mimics. Coast Eng 117:70–78. <https://doi.org/10.1016/j.coastaleng.2016.07.004>
- Potapova-Crighton O (2003) Torness Power station—hydrographic survey for the tidal discharge. Tidal Waters. SEPA
- Seelam JK, Guard PA, Balbock TE (2011) Measurement and modeling of bed shear stress under solitary waves. Coast Eng 58(9):937–947
- Spanakis N, Rogers BD, Stansby PK, Lenas A (2014) Modelling of seaweed ingress into a nuclear power station cooling water intake, 21st Telemac & Mascaret User Club, Grenoble
- Thomsen MS (2004) Species, thallus size and substrate determine macroalgal break force and break location in a low-energy soft-bottom lagoon. Aquat Bot 80:153–161. <https://doi.org/10.1016/j.aquabot.2004.08.002>
- Utter BD, Denny MW (1996) Wave-induced forces of the giant kelp *Macrocystis Pyrifera* (agardh): field test of a computational model. J Exp Biol 199:2645–2654
- Wernberg T, Thomsen MS (2005) The effect of wave exposure on the morphology of *Ecklonia radiata*. Aquat Bot 83:61–67. <https://doi.org/10.1016/j.aquabot.2005.05.007>

Publisher's Note Springer Nature remains neutral with regard to jurisdictional claims in published maps and institutional affiliations.